# Controlling Spin Relaxation in Hexagonal BN-Encapsulated Graphene with a Transverse Electric Field

M. H. D. Guimarães,* P. J. Zomer, J. Ingla-Aynés, J. C. Brant, N. Tombros, and B. J. van Wees
*Physics of Nanodevices, Zernike Institute for Advanced Materials, University of Groningen, Nijenborgh 4, 9747 AG, Groningen, The Netherlands*

(Received 2 June 2014; published 22 August 2014)

We experimentally study the electronic spin transport in hexagonal BN encapsulated single layer graphene nonlocal spin valves. The use of top and bottom gates allows us to control the carrier density and the electric field independently. The spin relaxation times in our devices range up to 2 ns with spin relaxation lengths exceeding 12 $\mu$m even at room temperature. We obtain that the ratio of the spin relaxation time for spins pointing out-of-plane to spins in-plane is $\tau_\perp/\tau_{||} \approx 0.75$ for zero applied perpendicular electric field. By tuning the electric field, this anisotropy changes to $\approx$0.65 at 0.7 V/nm, in agreement with an electric field tunable in-plane Rashba spin-orbit coupling.

DOI: 10.1103/PhysRevLett.113.086602 PACS numbers: 72.80.Vp, 72.25.-b, 85.75.Hh

The generation, manipulation, and detection of spin information has been the target of several studies due to the implications for novel spintronic devices [1,2]. In recent years, graphene has attracted a lot of attention in spintronics due to its theoretically large intrinsic spin relaxation time and length of the order of $\tau_s \approx 100$ ns and $\lambda_s \approx 100$ $\mu$m, respectively [3,4]. Although experimental results still fall short of these expectations [5–8], graphene has already achieved the longest measured nonlocal spin relaxation length [6,9] and furthest transport of spin information at room temperature [10]. However, the mechanisms for spin relaxation in graphene are still under heavy debate with various theoretical models proposed [3,4,11–14].

To take advantage of the long spin relaxation times in graphene, e.g., for spin logic devices, one requires easy control of the spin information, e.g., by an applied electric field. Single layer graphene is an ideal system for this purpose, not only because of its high mobilities and low intrinsic spin-orbit fields (SOFs), but also due to the simple relation between the carriers' wave vector, the applied perpendicular electric field, and the induced Rashba SOF [3,4,15–20]. In bilayer graphene, a more complicated behavior is expected when spin-orbit coupling is considered [21].

Here, we report nonlocal spin transport measurements on single layer graphene in which we address both topics specified above. Our devices consist of a single layer graphene flake on hexagonal boron nitride (h-BN) of which a central region is encapsulated with another h-BN flake and, hence, protected from the environment. The presence of a top gate (tg) and bottom gate (bg) give rise to two independent electric fields that are experienced by the graphene $E_{\mathrm{tg}} = -\epsilon_{\mathrm{tg}}(V_{\mathrm{tg}} - V^0_{\mathrm{tg}})/d_{\mathrm{tg}}$ and $E_{\mathrm{bg}} = \epsilon_{\mathrm{bg}}(V_{\mathrm{bg}} - V^0_{\mathrm{bg}})/d_{\mathrm{bg}}$, respectively [22], where $\epsilon_{\mathrm{tg(bg)}} \approx 3.9$ is the dielectric constant, $d_{\mathrm{tg(bg)}}$ is the dielectric thickness, and $V^0_{\mathrm{tg(bg)}}$ the position of the charge neutrality point for the top (bottom) gate. Their difference controls the carrier density in the graphene $[n = (E_{\mathrm{bg}} - E_{\mathrm{tg}})\epsilon_0/e]$ and their average gives the effective electric field experienced by the graphene $[\bar{E} = (E_{\mathrm{tg}} + E_{\mathrm{bg}})/2]$, which breaks the inversion symmetry in the encapsulated region, where $\epsilon_0$ is the electric constant and $e$ the electric charge. Our devices show enhanced spin relaxation times of at least 2 ns and, also, due to the higher electronic mobility, spin relaxation lengths above 12 $\mu$m at room temperature (RT) and 4.2 K. By a simple model we show that the measured spin relaxation times are a lower bound due to the influence of the nonencapsulated regions.

By comparing the spin relaxation time for spins out of plane ($\tau_\perp$) to spins in plane ($\tau_{||}$) as a function of the electric field, we get insight on the nature of the SOFs that cause spin relaxation in graphene. For SOFs pointing preferentially in the graphene plane, e.g., for adatoms and impurities, we expect $\tau_\perp \approx 0.5\tau_{||}$ [2,3,20,23]. If the SOFs point out of plane, as for ripples [3], we have $\tau_\perp \gg \tau_{||}$. However, if the main relaxation mechanism is through random magnetic impurities or defects, no preferential direction for the spins is expected $\tau_{||} \approx \tau_\perp$. Here, we obtain $\tau_\perp/\tau_{||} \approx 0.75$ at $\bar{E} = 0$ V/nm$^{-1}$. This ratio decreases with increasing $\bar{E}$, in agreement with an electric field induced Rashba SOF pointing in the graphene plane.

Device number 1 is illustrated in Figs. 1(a) and 1(b). The h-BN-graphene-h-BN stack sits on a 300 nm thick $SiO_2$ layer on a heavily doped Si substrate which is used as a backgate. The sample preparation is described in detail in the Supplemental Material [24] and follows Refs. [25,26]. We use Co electrodes with a thin $TiO_2$ interface barrier to perform spin transport measurements. Three devices were studied, all showing similar results. Here, we show the results for the device with the longest encapsulated region ($\approx$12 $\mu$m) and spacing between the inner contacts (13.8 $\mu$m).

The charge transport properties of the encapsulated region are measured by applying a current between

 © 2014 American Physical Society

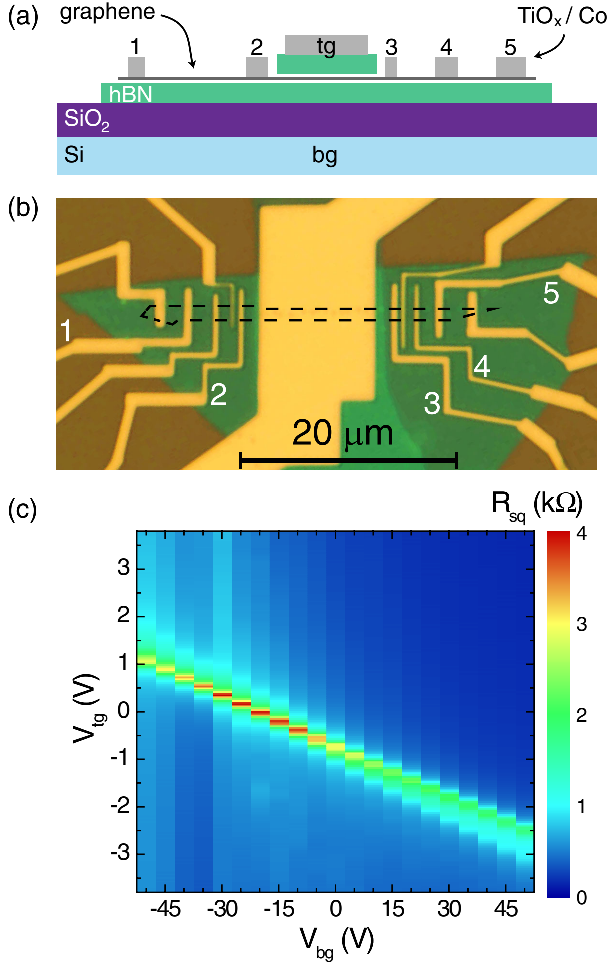


FIG. 1 (color online). (a) Side-view schematics and (b) top-view optical microscope image of a h-BN encapsulated graphene spin valve. The numbers show the contact electrodes, and the top (bottom) gate electrodes are indicated as tg (bg). The graphene is outlined by the dashed line. (c) Square resistance ($R_{sq}$) as a function of $V_{tg}$ and $V_{bg}$.

electrodes 1 and 5, Figs. 1(a) and 1(b), and scanning the top and bottom gate voltages ($V_{tg}$ and $V_{bg}$, respectively) while recording the voltage between electrodes 2 and 3. Figure 1(c) shows the square resistance ($R_{sq}$) as a function of $V_{tg}$ and $V_{bg}$. The charge neutrality point depends on both $V_{tg}$ and $V_{bg}$ in a linear fashion. The slope of the line gives the ratio between the bottom and top gate capacitances $\alpha_{bg}/\alpha_{tg} \approx 0.036$. A small top gate independent resistance peak around $V_{bg} = -16.6$ V [not visible in Fig. 1(c)] arises from the non-top-gated regions between the two inner contacts. The electronic mobility for this device is $\mu \approx 1.5$ m$^2$/V s at RT and $\mu \approx 2.3$ m$^2$/V s at 4.2 K. Although the mobilities of our devices are above the best devices based on $SiO_2$, they are still 1 order of magnitude lower than the best devices on h-BN [25] which can be attributed to small bubbles or contamination visible on the graphene/h-BN stack.

Spin dependent measurements are performed using a standard nonlocal geometry in which the current path is separated from the voltage detection circuit [5]. The current is driven between electrodes 1 and 2 and the voltage measured between electrodes 3 and 5, which are on the other side of the encapsulated region [Figs. 1(a) and 1(b)]. To obtain the spin relaxation time ($\tau_s$) and the spin diffusion coefficient ($D_s$) we perform Hanle precession measurements where the nonlocal signal is measured as a function of a perpendicular magnetic field $B$. We then fit the data with the solution to the Bloch equations [5].

The results for $D_s$, $\tau_s$, and the spin relaxation length ($\lambda_s = \sqrt{D_s \tau_s}$) as a function of the $V_{tg}$ for three values of $V_{bg}$ at 4.2 K are shown in Fig. 2. A similar set of measurements was performed at RT and for other samples where only a small difference was observed (see Supplemental Material [24]).

Because of our device mobility, $D_s$ is higher than for regular graphene devices on $SiO_2$ ($D_s \approx 0.02$ m$^2$/s) [5,6] and comparable to suspended [8] and nonencapsulated h-BN supported devices [10] ($D_s \approx 0.05$ m$^2$/s). As an extra confirmation, we check that $D_s$ agrees with the charge diffusion coefficient $D_c = [R_{sq} e^2 \nu(E_F)]^{-1}$ [27], where $e$ is the electron charge and $\nu(E_F)$ the density of states at the Fermi energy $E_F$. Next, we observe that the obtained spin relaxation times are higher than those on regular $SiO_2$ substrates ($\tau_s \approx 0.1$–$1$ ns) [5,6] and in nonencapsulated h-BN supported devices ($\tau_s \approx 0.1$–$0.5$ ns) [10], reaching up to $\tau_s = (1.9 \pm 0.2)$ ns at 4.2 K and $\tau_s = (2.4 \pm 0.4)$ ns for RT. These values surpass all previous nonlocal measurements of $\tau_s$ in single layer graphene both at room and low temperatures [28,29]. We obtain a maximum of $\lambda_s = 12.3$ $\mu$m at 4.2 K and $\lambda_s = 12.1$ $\mu$m at RT.

Comparing $\tau_s$ obtained in our devices with nonencapsulated h-BN based devices ($\tau_s \approx 0.2$ ns) [10], we can conclude that the encapsulation of graphene on h-BN significantly increases the spin relaxation times. Note that the nonencapsulated devices had comparable electronic mobilities which indicates that $\tau_s$ is not linked to the momentum relaxation time in a trivial manner [30]. By measuring a region about 5 $\mu$m away from the encapsulated part, we find $D_s \approx 0.03$ m$^2$/s, $\tau_s \approx 0.3$ ns, and $\lambda_s \approx 3$ $\mu$m, in agreement with the previously reported results. The increase in $\tau_s$ for the encapsulated region can be due to several factors. This region is protected from polymer remains or other contamination which can increase spin scattering. In addition to that, the inversion asymmetry, which can generate an extra term for the spin-orbit coupling, is also reduced and controlled by tuning $V_{tg}$ and $V_{bg}$ separately as explained earlier.

As can be seen in Fig. 2, $\tau_s$ is modulated by $V_{tg}$, showing a dip close to the charge neutrality point in the encapsulated region (e.g., $V_{tg} = 1.1$ V and $V_{bg} = -52.5$ V). For larger charge carrier densities in the nonencapsulated regions, the modulation in $\tau_s$ by $V_{tg}$ is smaller, although still present.

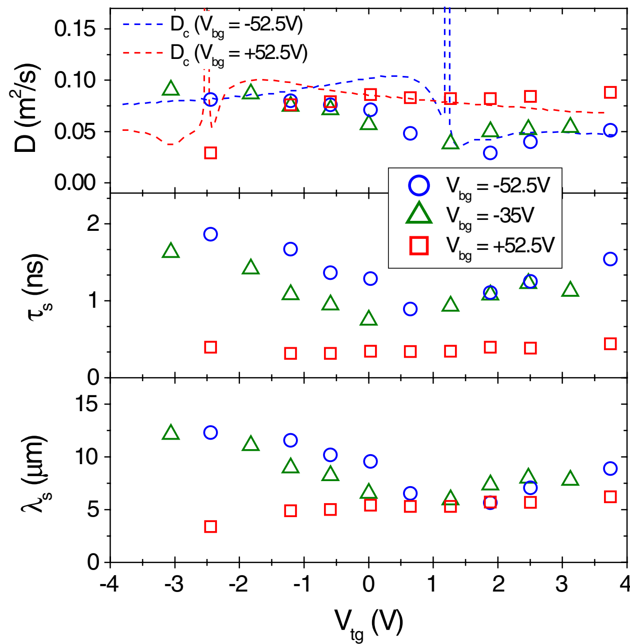


FIG. 2 (color online). (Spin) diffusion coefficient ($D_s$), spin relaxation time $\tau_s$, and spin relaxation length $\lambda_s$ as a function of $V_{tg}$ for three different values of $V_{bg}$. The error bars are smaller than the dot size. The dashed red (blue) lines show the charge diffusion coefficient $D_c$ for $V_{bg} = +52.5$ V($-52.5$ V).

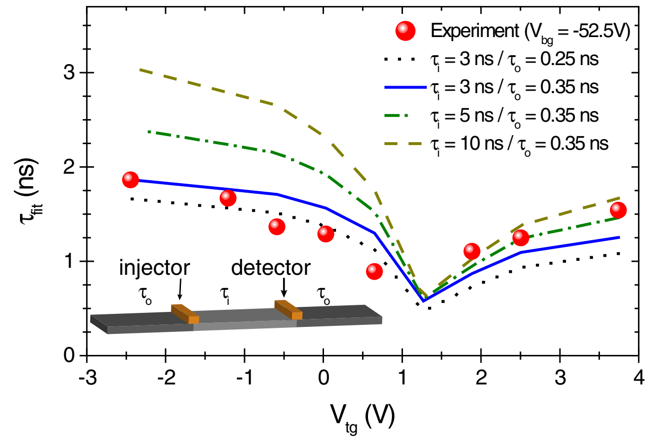


FIG. 3 (color online). Effective spin relaxation times extracted for different values for $\tau_o$ and $\tau_i$ (lines) compared to our experimental data for $V_{bg} = -52.5$ V (dots). The inset shows a schematic of the simulated system.

Furthermore, the average value of $\tau_s$ is maximum at low carrier densities in the nonencapsulated regions (large negative $V_{bg}$) and decreases with increasing $V_{bg}$. This difference on the measured $\tau_s$ for different carrier densities on the outer regions can be explained by simulations that treat the full device [8]. Since the transport is diffusive, the spins can explore both the encapsulated and the non-encapsulated regions before being detected. We take this into account by describing our sample as two outer regions connected by a central region [24]. The relevant parameters ($R_{sq}$, $D_s$, and $\tau_s$) are set for each region individually. The values for the outer regions and $R_{sq}$ and $D_s$ for the inner region can be extracted from our charge and spin transport measurements.

Changing the values of the spin relaxation time for the outer regions, $\tau_o$, around the experimentally obtained values and changing the values for the spin relaxation time in the inner region, $\tau_i$, we simulate Hanle precession curves that are fitted in the same way done for our experiments to obtain an effective value for the spin relaxation time $\tau_{fit}$. We get a reasonable quantitative agreement between our simulations and experiment at $V_{bg} = -52.5$ V for $\tau_i = 3$ ns (Fig. 3). This means that the spin relaxation time for the encapsulated region is higher ($\tau_s \approx 3$ ns), but still within the same order of magnitude as the values obtained by analyzing the data using a homogeneous system (Fig. 2). The trend in $V_{tg}$ is also reproduced, which indicates that it is given by the ratio of the resistivities of the inner and outer regions.

Even though the experimentally obtained value for $\tau_s$ depends on the gate voltages in a nontrivial way due to the influence of the nonencapsulated regions, we can still study how the electric field affects the ratio between the spin relaxation times for out-of-plane to in-plane spins $r = \tau_\perp/\tau_{||}$. As explained in the introduction, this way we can get insight about the SOFs in our system.

To compare the spin relaxation for spins parallel and perpendicular to the graphene plane, we perform the Hanle precession measurements as described before, but increase the perpendicular magnetic field to higher values, $B > 1$ T. At such high magnetic fields, the magnetization of the electrodes rotates out of plane and the injected spins do not precess anymore. This is seen as a saturation of the nonlocal signal at high B, Fig. 4(a).

We observe that different combinations of $V_{tg}$ and $V_{bg}$ result in a saturation of $R_{nl}$ at high magnetic fields at values always smaller than $R_{nl}$ at $B = 0$ T, with the saturation occurring at 43%–57% of the initial value. Given that the nonlocal spin signal is given by $\Delta R_{nl} = (P^2 R_{sq}\lambda_s/W)e^{-L/\lambda_s}$, where $P$ is the polarization of the electrodes, $L$ the distance between electrodes, and $W$ the channel width, we can estimate the anisotropy in the spin relaxation times assuming that $P$ and $R_{sq}$ do not change significantly with field. Because of a large magnetoresistance at low carrier densities, our analysis is done only for points at large enough carrier densities for both the inner and outer regions [31]. We can relate the ratio of the nonlocal spin signal and the ratio of the spin relaxation times by $R_{nl}^{\perp}/R_{nl}^{||} = \sqrt{r}e^{(L/\lambda_{||})(\sqrt{r}-1/\sqrt{r})}$, where $\lambda_{||} = \sqrt{D_s\tau_{||}}$ is obtained via our Hanle precession measurements. In Fig. 4(b), we plot the ratio $\tau_\perp/\tau_{||}$ as a function of $\bar{E}$ for different values of $n$ where we see a clear decrease of this ratio, from 0.75 at $\bar{E} \approx 0$ V/nm to about 0.65 at $\bar{E} \approx -0.7$ V/nm. The inset of Fig. 4(b) shows the dependence of $r$ as a function of $n$ for different values of $\bar{E}$ where no clear trend can be seen. The

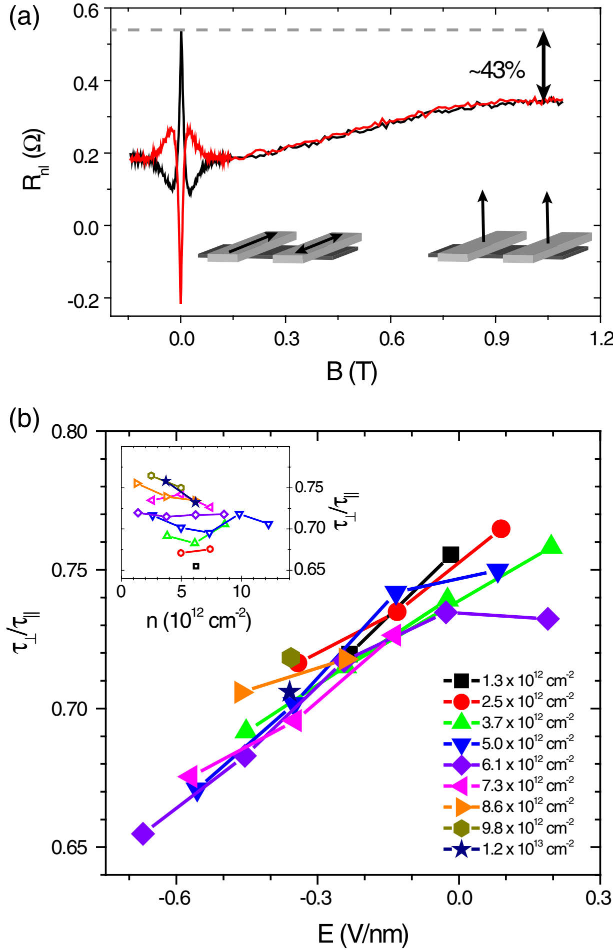


FIG. 4 (color online). (a) $R_{nl}$ as a function of $B$ showing Hanle precession at low fields and a saturation of the signal at high fields when the magnetization of the electrodes point out of plane. Inset: A cartoon showing the magnetization of the contacts: in plane at low fields and out of plane at high fields. (b) The ratio $\tau_\perp/\tau_{||}$ as a function of electric field $\bar{E}$ for different values of carrier density $n$. Inset: The same data points for $\tau_\perp/\tau_{||}$ used in the main graph, but plotted as a function of $n$ where different colors and symbols represent the different values of $\bar{E}$.

value for $\tau_\perp/\tau_{||}$ for zero electric field is similar to the values found previously on $SiO_2$ based devices ($\tau_\perp \approx 0.8\tau_{||}$) [23]. In the case of an inversion symmetric graphene layer with no extrinsic sources for SOFs, we would not expect any particular preference for direction of the spins, meaning that $\tau_\perp \approx \tau_{||}$ [2]. The fact that even at $\bar{E} = 0$ V/nm the ratio between $\tau_\perp$ and $\tau_{||}$ is below 1 means that, even without an externally applied electric field, there are probably remanent SOFs pointing preferentially in the graphene plane.

The decrease of $r$ with increasing $\bar{E}$ is in agreement with theories that dictate an increase in in-plane Rashba SOF with the increase of electric field [4,15–20]. The Rashba-type spin-orbit Hamiltonian for graphene is given by $\mathcal{H}_{SO} = \Delta_R/2(\boldsymbol{\sigma} \times \mathbf{s})_z$, where $\boldsymbol{\sigma}$ and $\mathbf{s}$ are the pseudospin and real spin Pauli matrices, respectively. For single layer graphene, the spin-orbit constant is known to depend on the $\bar{E}$ in a linear way $\Delta_R = \zeta\bar{E}$ [15,19], where $\zeta$ is the coupling constant. Theoretical values range from $\zeta = 0.3$–$66\ \mu$eV/V nm$^{-1}$ [15–18]. We can roughly estimate $\zeta$ by assuming a D'Yakonov-Perel mechanism for spin relaxation [20,32] with different values for the spin orbit coupling for in- and out-of-plane spins. Our analysis [24] results in $\zeta \approx (40 \pm 20)\ \mu$eV/V nm$^{-1}$, within the range of the theoretical predictions.

In conclusion, we measured the spin transport characteristics of a single layer graphene device encapsulated with h-BN. We measured spin relaxation times up to $\tau_s \approx 2$ ns and spin relaxation lengths above $\lambda_s = 12\ \mu$m. By taking into consideration that the nonencapsulated regions of our devices play a role in our measurements of $\tau_s$, we estimate the actual spin relaxation time in the encapsulated region to be $\tau_s \approx 3$ ns. Furthermore, we showed that the ratio between out-of-plane and in-plane spin relaxation times changes from $\tau_\perp/\tau_{||} \approx 0.75$ to 0.65 with increasing the applied out-of-plane electric field. This observation is in agreement with an electric field induced Rashba-type spin orbit field. Our results show not only that $\tau_s$ in graphene can be improved by improving the quality of the devices, but also that electrical control of spin information in graphene is possible, paving the way to new graphene spintronic devices.

We would like to acknowledge A. Kamerbeek and E. Sherman for insightful discussions and J. G. Holstein, H. M. de Roosz, and H. Adema for the technical support. The research leading to these results has received funding from the Dutch Foundation for Fundamental Research on Matter (FOM), the European Union Seventh Framework Programme under Grant Agreement No. 604391 Graphene Flagship, the People Programme (Marie Curie Actions) of the European Union's Seventh Framework Programme No. FP7/2007-2013/ under REA Grant Agreement No. 607904-13 Spinograph, NWO, NanoNed, the Zernike Institute for Advanced Materials, and CNPq, Brazil.

*Note added.*—Recently, we became aware of a work in which $\lambda_s$ up to 10 $\mu$m for single and few-layer graphene were achieved for a single gated structure which did not allow the study of $\tau_s$ as a function of $\bar{E}$ [33].

*m.h.diniz.guimaraes@rug.nl

[1] S. A. Wolf, D. D. Awschalom, R. A. Buhrman, J. M. Daughton, S. von Molnr, M. L. Roukes, A. Y. Chtchelkanova, and D. M. Treger, Science **294**, 1488 (2001).
[2] J. Fabian, A. Matos-Abiague, C. Ertler, P. Stano, and I. Zutic, Acta Phys. Slovaca **57**, 565 (2007).
[3] D. Huertas-Hernando, F. Guinea, and A. Brataas, Phys. Rev. Lett. **103**, 146801 (2009).

[4] V. K. Dugaev, E. Y. Sherman, and J. Barnaś, Phys. Rev. B **83**, 085306 (2011).
[5] M. Popinciuc, C. Józsa, P. J. Zomer, N. Tombros, A. Veligura, H. T. Jonkman, and B. J. van Wees, Phys. Rev. B **80**, 214427 (2009).
[6] W. Han and R. K. Kawakami, Phys. Rev. Lett. **107**, 047207 (2011).
[7] T.-Y. Yang, J. Balakrishnan, F. Volmer, A. Avsar, M. Jaiswal, J. Samm, S. R. Ali, A. Pachoud, M. Zeng, M. Popinciuc, G. Güntherodt, B. Beschoten, and B. Özyilmaz, Phys. Rev. Lett. **107**, 047206 (2011).
[8] M. H. D. Guimarães, A. Veligura, P. J. Zomer, T. Maassen, I. J. Vera-Marun, N. Tombros, and B. J. van Wees, Nano Lett. **12**, 3512 (2012).
[9] M. Wojtaszek, I. J. Vera-Marun, T. Maassen, and B. J. van Wees, Phys. Rev. B **87**, 081402 (2013).
[10] P. J. Zomer, M. H. D. Guimarães, N. Tombros, and B. J. van Wees, Phys. Rev. B **86**, 161416 (2012).
[11] D. Kochan, M. Gmitra, and J. Fabian, Phys. Rev. Lett. **112**, 116602 (2014).
[12] P. Zhang and M. W. Wu, New J. Phys. **14**, 033015 (2012).
[13] S. Roche and S. O. Valenzuela, J. Phys. D **47**, 094011 (2014).
[14] H. Ochoa, A. H. Castro Neto, and F. Guinea, Phys. Rev. Lett. **108**, 206808 (2012).
[15] M. Gmitra, S. Konschuh, C. Ertler, C. Ambrosch-Draxl, and J. Fabian, Phys. Rev. B **80**, 235431 (2009).
[16] D. Huertas-Hernando, F. Guinea, and A. Brataas, Phys. Rev. B **74**, 155426 (2006).
[17] C. L. Kane and E. J. Mele, Phys. Rev. Lett. **95**, 226801 (2005).
[18] H. Min, J. E. Hill, N. A. Sinitsyn, B. R. Sahu, L. Kleinman, and A. H. MacDonald, Phys. Rev. B **74**, 165310 (2006).
[19] E. I. Rashba, Phys. Rev. B **79**, 161409 (2009).
[20] C. Ertler, S. Konschuh, M. Gmitra, and J. Fabian, Phys. Rev. B **80**, 041405 (2009).
[21] S. Konschuh, M. Gmitra, D. Kochan, and J. Fabian, Phys. Rev. B **85**, 115423 (2012).
[22] Y. Zhang, T.-T. Tang, C. Girit, Z. Hao, M. C. Martin, A. Zettl, M. F. Crommie, Y. R. Shen, and F. Wang, Nature (London) **459**, 820 (2009).
[23] N. Tombros, S. Tanabe, A. Veligura, C. Jozsa, M. Popinciuc, H. T. Jonkman, and B. J. van Wees, Phys. Rev. Lett. **101**, 046601 (2008).
[24] See Supplemental Material at http://link.aps.org/supplemental/10.1103/PhysRevLett.113.086602 for a detailed description of the device fabrication, transport measurements, simulation of spin transport in inhomogeneous systems, analysis of the experimental data, results for different samples and temperatures, and the estimation of the electric field dependent spin-orbit coupling.
[25] L. Wang, I. Meric, P. Y. Huang, Q. Gao, Y. Gao, H. Tran, T. Taniguchi, K. Watanabe, L. M. Campos, D. A. Muller, J. Guo, P. Kim, J. Hone, K. L. Shepard, and C. R. Dean, Science **342**, 614 (2013).
[26] P. J. Zomer, M. H. D. Guimarães, J. C. Brant, N. Tombros, and B. J. van Wees, Appl. Phys. Lett. **105**, 013101 (2014).
[27] A resistance of 3.2 kΩ was subtracted in the calculation of $D_c$ for $V_{\mathrm{bg}} = -52.5$ V to account for the non-top-gated regions.
[28] Two-terminal local measurements on epitaxial graphene estimated $\tau_s \approx 100$ ns at 4.2 K [29].
[29] B. Dlubak, M.-B. Martin, C. Deranlot, B. Servet, S. Xavier, R. Mattana, M. Sprinkle, C. Berger, W. A. De Heer, F. Petroff, A. Anane, P. Seneor, and A. Fert, Nat. Phys. **8**, 557 (2012).
[30] W. Han, J.-R. Chen, D. Wang, K. M. McCreary, H. Wen, A. G. Swartz, J. Shi, and R. K. Kawakami, Nano Lett. **12**, 3443 (2012).
[31] At low $n$, $R_{\mathrm{sq}}$ of our devices scales with $\mathrm{B}^2$ leading to a background in our signal that overcomes the nonlocal spin signal at large B.
[32] M. D'Yakonov and V. Perel', Sov. Phys. JETP **33**, 1053 (1971).
[33] M. Drogeler, F. Volmer, M. Wolter, B. Terres, K. Watanabe, T. Taniguchi, G. Guntherodt, C. Stampfer, and B. Beschoten, arXiv:1406.2439.